An Integrated CNC Accumulation System for Automatic Building-around-inserts

Xuejin Zhao[a,b], Yayue Pan[a], Chi Zhou[a], Yong Chen[a]*, Charlie C. L. Wang[c]

[a]Epstein Department of Industrial and Systems Engineering
University of Southern California, Los Angeles, CA, USA

[b]School of Mechanical Engineering, Shandong University, Ji'nan, Shandong, China

[c]Department of Mechanical and Automation Engineering
The Chinese University of Hong Kong, Hong Kong, China

*Corresponding author: yongchen@usc.edu, (213) 740-7829

ABSTRACT
In this paper a non-layer-based *additive manufacturing* (AM) process named *computer numerically controlled* (CNC) accumulation process is presented for applications such as plastic part repairing and modification. To facilitate the AM process, a novel *three-dimensional* (3D) laser scanning system based on a *micro-electo-mechanical system* (MEMS) device is developed for *in situ* scanning of inserted components. The integration of the scanning system in the CNC accumulation process enables the building-around-inserts with little human efforts. A point processing method based on the *algebraic point set surface* (APSS) fitting and *layered depth-normal image* (LDNI) representation is developed for converting the scanning points into triangular meshes. The newly developed 3D scanning system is compact with sufficient accuracy for the CNC accumulation process. Based on the constructed base surface model, data processing operations including multi-axis tool path planning and motion control are also investigated. Multiple test cases are performed to illustrate the capability of the integrated CNC accumulation process on addressing the requirements of building-around-inserts.

KEYWORDS
Additive manufacturing, building around insert, CNC accumulation, 3D scanning, process planning.

1. INTRODUCTION

Manufacturing processes can be generally classified into additive-based, subtractive-based, and deformation-based processes [1]. Each process has its own unique capability in addressing requirements such as shapes, materials, speed, cost, quantity, accuracy, flexibility, etc. To take advantage of different manufacturing processes, it is desired for future manufacturing processes to have the capability of *building-around-inserts*. That is, the process is capable of incorporating existing components that are fabricated by other manufacturing processes in the fabrication process [2, 3]. Such capability, if fully realized, would enable new product components with heterogeneous material properties and multi-functionality be developed for future engineering systems.

Over the past twenty-five years, a collection of *additive manufacturing* (AM) processes have been developed for the need of direct digital manufacturing. A unique capability of AM processes is that they can fabricate parts directly from *computer-aided design* (CAD) models without part-specific tooling or fixtures. Current AM processes are mostly planar-layer-based, that is, materials are accumulated based on uniform layer-by-layer deposition in a single building direction. While the planar layers make the algorithm development, software coding, and hardware implementation simpler, the allowable motion between the tool and the work piece is limited. In most cases, only translational motions in the *X*, *Y*, and *Z* axes are allowed in AM processes, e.g. *Stereolithography apparatus* (SLA) and *selective laser sintering* (SLS). Consequently, embedding existing components in such processes is usually difficult. For example, Kataria and Rosen [2] identified some major problems related to building-around-inserts in the SLA process including laser shadowing and vat recoating. Both of the problems are related to the uniform layer-based fabrication approach.

Recently a non-layer-based AM process named the *Computer Numerically Controlled* (CNC) *accumulation* process was developed [4]. The tool path of the CNC accumulation process can have multi-axis motions; consequently, the CNC accumulation process is flexible in incorporating existing components in the building process.

Multi-axis CNC Accumulation Process

Similar to AM processes such as the laser- or DMD-based SLA processes [5, 6], the CNC accumulation process [4] is based on selectively curing photocurable resin. However, different from the SLA process, the curing tool in the CNC accumulation process is merged in liquid resin. Hence the tool can cure resin in various orientations with unconstrained material feeding. A critical problem to be addressed in the CNC accumulation process is how to ensure the newly cured resin will attach to the base or previously built part instead of the accumulation tool. In our previous work [4], the attaching forces in the CNC accumulation process were studied. The feasibility of the CNC accumulation process has been demonstrated based on: (1) applying certain type of coating (e.g. Teflon film) on the tip of the curing tool such that the attaching force between the resin and the tool can be reduced; and (2) ensuring adequate over curing of liquid resin such that the attaching force between the newly cured resin and the base or the previously built part will be sufficiently large.

The CNC accumulation process has great similarity to the CNC machining process. As shown in Figure 1a, the CNC machining process uses a machining tool to remove the material that is in touch with the subtracting tool. Hence, for a given work piece (W) and tool path (S_i) with tool orientation in each cutter location (O_j), the constructed shape (M) will be $M = W - \bigcup(T)_{S_i+O_j}$. In contrast, the CNC accumulation process, as shown in Figure 1b, uses an accumulation tool to add material that is in touch with the curing tool. Hence, for tool path (S_i) with tool orientation (O_j), the constructed shape (M) will be $M = \bigcup(T)_{S_i+O_j}$.

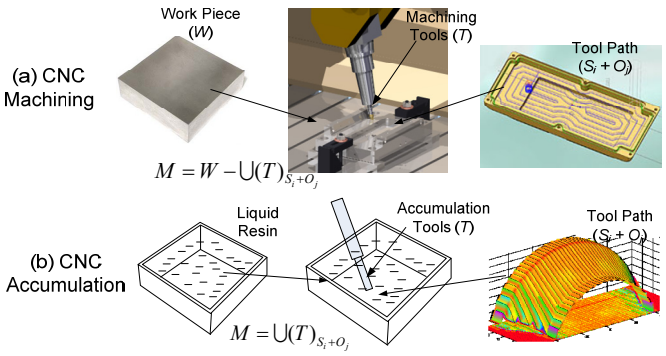

Figure 1: A comparison of (a) the CNC machining and (b) the CNC accumulation processes [4].

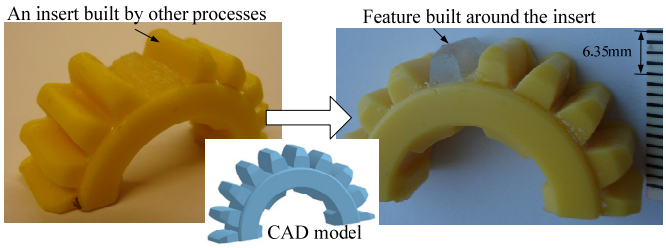

Figure 2: A comparison of the CNC machining and accumulation processes.

Two good properties of the CNC accumulation process are: (1) The allowable motions between the tool and the work piece are significantly increased; and (2) the feeding of liquid resin to facilitate the material accumulation process is straightforward since a tool is merged in liquid resin during the building process.

Automatic Building-around-inserts

The feasibility of using the CNC accumulation process in applications such as building-around-inserts has been demonstrated [4]. A critical challenge identified in our previous study is how to generate tool paths for an inserted component whose digital model and relative position are unknown. Similar to the CNC machining process, the collision between tools and workpiece needs to be identified and avoided in the tool path planning of the CNC accumulation process. In addition, an appropriate gap between the tool tip and the base surface needs to be set to ensure the newly cured resin will not attach to the accumulation tool [4].

Figure 2 shows a test case based on a gear with a broken tooth. Suppose the plastic gear is fabricated by the injection molding or other AM processes and one of the teeth is broken. Instead of throwing it away, the broken gear can be repaired using the CNC accumulation process. However, the tool path planning for adding the desired tooth can be challenging since (1) the physical object to be repaired may be positioned arbitrarily on the platform; (2) the surface of the broken tooth, which will be used as the base surface for the missing tooth, can be irregular.

Hence, a critical challenge in using the CNC accumulation process in building-around-inserts is to automate the tool path planning for any given objects to be built on. If successfully addressed, the capability of remanufacturing parts will not only reduce the material and energy waste, but also expand the functionality of product components. Additive manufacturing processes such as Tungsten Inert Gas (TIG) welding and Laser Engineered Net Shaping (LENS) have been developed for repairing and modifying metallic parts; however, automatic repairing and modification processes for plastic parts are still lacking. Such product sustainability issues attract increasing attentions in recent years. We are motivated to develop the CNC accumulation process in addressing such needs.

Contributions

To increase the capability of the CNC accumulation process in building-around-inserts, an *in situ* scanning system that can capture the shape of inserted objects and related geometric processing methods are developed for the multi-axis CNC accumulation process. Test results indicate that the accuracy of the developed 3D scanner is satisfactory. A set of geometric processing methods have also been presented including the APSS point processing, LDNI-based surface retrieving and offsetting, G-code tool

path planning, and 5-axis accumulation motion control. Experimental results verify the capability of the integrated CNC accumulation system in building-around-inserts. The process may offer an effective and efficient fabrication process for plastic part repairing and modification.

2. AN INTEGRATED CNC ACCUMULATION SYSTEM

Various 3D scanning systems have been developed before and commercially available. Although the scanners can be used in generating the digital model of an insert component, such an *ex situ* scanning approach will require additional effort on registering the position and orientation of the component inside the tank. In comparison, an *in situ* 3D scanner that is integrated in the CNC accumulation system can directly capture the geometric information of a base surface related to accumulation tools. Hence the tool paths for building given shapes on the surface can be quickly planned.

A desired *in-situ* 3D scanner needs to be compact on size and flexible on accommodating the position or orientation of a mounted component in the tank. It also needs to have sufficient accuracy for the CNC accumulation process. In addition, the scanning process is desired to require little or no human involvement such as adding markers, or constantly registering the position of the scanner related to the tank. Another important consideration in selecting a 3D scanning approach is that only the concerned surface model needs to be captured in order to enable to use the CNC accumulation process in building around inserts. There is no need to reconstruct the 3D model of the whole object.

Current 3D scanning systems can be classified into contact and non-contact systems. The contact 3D scanners use a probe to physically touch the surface of an object. In addition to a firm fixture for holding the object, a motion system is needed to translate and orient the touch probe related to the surface. In comparison, non-contact 3D scanners emit radiation or light beams, and use detectors to receive the signals refelected from the object [7]. A triangulation method is one of the most commonly used 3D scanning approaches [8]. In the triangulation method, a prepared light pattern is projected onto a surface in order to capture the point positions on the surface. The light pattern can be a dots, lines, or grids. A camera or light detector is then used to capture the projected light. Consequently, the 3D coordinates of the projected light on the surface can be calculated by a triangulation model [8].

Figure 3 shows a typical 3D scanning head based on the triangulation method. Both the laser and sensor are fixed inside the head. Some scanners have a rotating hexagon mirror to convert a laser dot into a laser line [9]. However, the limited freedom of the laser scanning path requires the use of an external motion system to translate the scanning head to cover a whole surface [9-12].

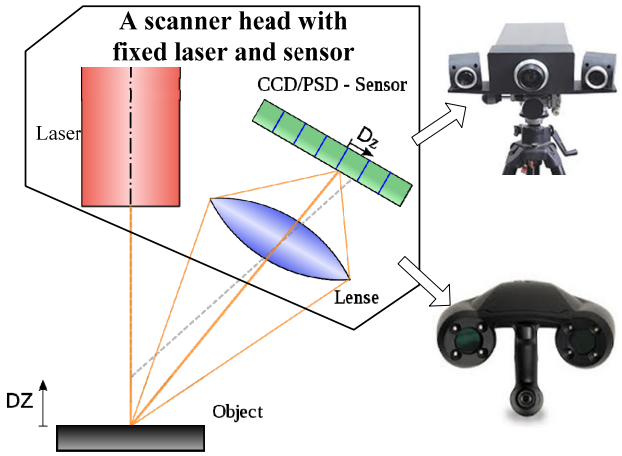

Figure 3: An illustration of the triangulation method and a scanning head with a fixed laser and sensor.

Micro-electo-mechanical systems (MEMS) is a rapidly growing, emerging technology. Products such as *direct digital micromirror* (DMD) devices have been used in AM processes [6, 13]. Recently a dual-axis analog MEMS pointing mirror device (TALP1000B), has been developed by Texas Instruments (Dallas, TX) [14]. The gold coated mirror (~3.2×3.6mm) of the MEMS device is constructed of single crystal silicon. It can be driven with precise pointing resolution. In addition, each rotation axis of the device is individually and independently controlled.

Such a compact dual-axis rotation mirror enables a laser dot to scan in a certin range. Hence it is possible to cover a surface by using the contorlled movement of such a micromirror instead of translating the scanning head that is much larger and more bulky. In this paper, a 3D scanner based on the MEMS technology is developed. An *in situ* scanning system based on it is compact, cheap and easy to be integrated. In addition, a base surface may be scanned with a single setup. Hence motion planning or data registering between multiple setups will not be required.

In the following sections, we will discuss the development of a 3D laser scanning system based on the dual-axis MEMS pointing mirror. The schematic design, prototype development and scanning point retrieval algorithms will be presented. The integration of the developed 3D scanner in a CNC accumulation system is also discussed. Based on the dual-axis mirror, the developed scanner returns scanning data of a surface portion where material needs to be added. The scanning result is usually sparse. Accordingly the algebraic point set surface (APSS) algorithm is adopted in processing the scanning points for constructing related surface models. Automatic tool path generation based on the scanning result is also presented. The data flow pipeline of an integrated CNC accumulation system for building-around-inserts is shown in Figure 4.

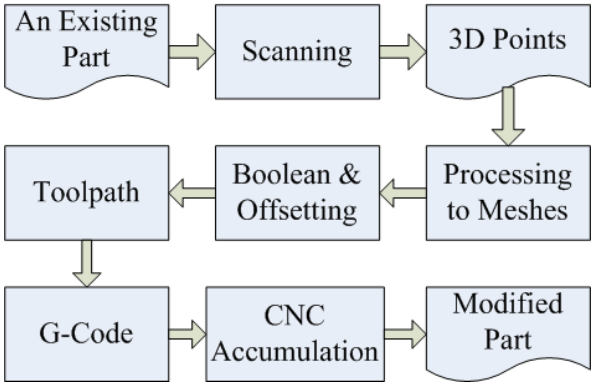

Figure 4: A pipeline of an integrated CNC accumulation system for automatic building-around-inserts.

The remainder of the paper is organized as follows. Section 3 presents the new laser scanner based on the MEMS device. Section 4 describes point processing algorithms for constructing the digital model of a scanning surface. Section 5 discusses the 5-axis tool path planning operations based on the scanning data. Two test cases are presented and analyzed in Section 6. Finally, conclusions from this study are drawn in Section 7.

3. DEVELOPMENT OF AN IN SITU 3D SCANNING SYSTEM

A dual-axis analog pointing mirror device (TALP1000B from Texas Instruments) has been identified as a potential solution for an *in situ* 3D scanner for the CNC accumulation process. With the use of a dual-axis mirror, a laser dot can scan along both the *X* and *Y* directions by tilting the mirror along the two axes (*NS* and *WE*). Different angle combinations of the mirror can reflect the laser dot to any position within a pre-defined scanning area. The moving freedom extended from a 1-dimensional (1D) line to a 2-dimensional (2D) area enables the scanning with no or little involvement of an external motion system.

Design of an Integrated 3D Scanning Unit

Figure 5 shows the schematic of a 3D scanning unit based on the dual-axis rotation mirror. A dot laser shoots a laser beam toward the mirror. The laser dot is then reflected by the mirror and shoots on the surface of a scanning object. By rotating the mirror along the *NS* and *WE* axes, the laser dot can scan any position within the scanning area. The scanning area that can be covered in one setup is dependent on the maximum rotation angles of the mirror ($\pm 5^{o}$). An appropriate scanning depth is determined by a calibration database. A camera is installed with the mirror to detect the laser dot reflected by the part surface. Based on the planned laser line and the captured image data, the 3D position of the intersection point can be calculated based on the aforementioned triangulation method.

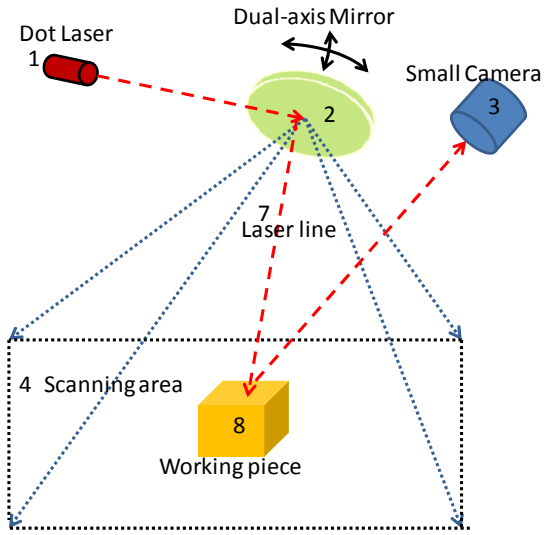

Figure 5: A schematic illustration of the dual-axis mirror based scanning unit.

Figure 6 shows a prototype laser scanner that is integrated into a 5-axis CNC accumulation system. In the 3D laser scanning unit, (1) a red dot laser by *LaserGlow Technologies* (Toronto, Canada) is selected based on the wavelength range of the coated mirror (700nm – 10μm). Its brightness and focus range can be adjusted. (2) The TALP1000B is a high-performance MEMS device designed for light steering applications. The rotation range of the two-axis mirror is ± 5 degrees and the mirror size is about 9mm^2. The switch time of the mirror is less than 5ms. The device provides position feedback with 13-bit resolution. (3) A small web camera with an image resolution of 640×480 is used as the light sensor.

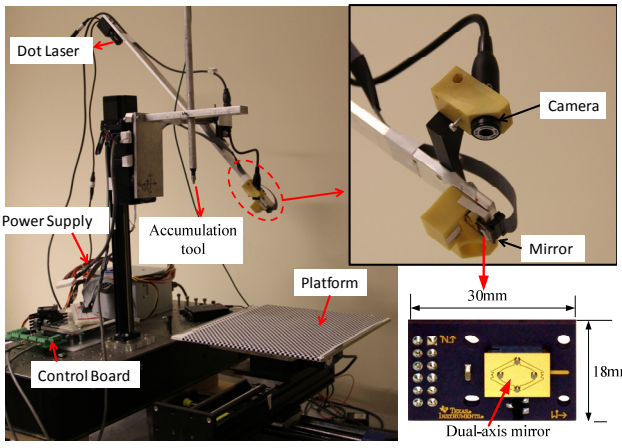

Figure 6: The setup of the 3D scanning unit with the dual-axis mirror in the 5-axis CNC accumulation system.

The dot laser and the dual-axis mirror are installed on the two ends of an aluminum bar. The laser dot reflected by the mirror falls on the platform, which is covered by a chessboard paper. Camera is installed side away from the mirror to capture the image of the reflected laser dot.

Other than the laser scanning unit, there are three translation stages *X*, *Y* and *Z*, and two rotation stages *A* and *B*. These five stages are designed for the 5-axis accumulation tool. A control board is used to control the movement of the 5 axis.

Based on such an integrated system, a given workpiece is first fixed in a resin tank that is placed on the platform. The laser scanning unit is then used to collect the scanning data related to the deposition surface. With the scanning data, tool paths for the accumulation process are computed using the point processing software and tool path generation operations. The accumulation tool, driven by the 5 axis motion stage, then adds material on the inserted workpiece.

The developed scanning unit can be mounted on a separate flexible arm. The unit can also be fixed on the motion system that is designed for the CNC accumulation tool. Consequently, the scanner can be moved up and down using the *Z* stage to enlarge the scanning volume in the *Z* direction, and moved sideways using the *X* and *Y* stages to enlarge the lateral scanning area.

For a fixed setup, as shown in Figure 5, the scanning area depends on the rotation angle of the dual-axis mirror, and the distance between mirror and the scanning plane. In addition, the camera image range needs to be larger than the laser scanning area. In the prototype system as shown in Figure 6, the defined scanning range has a *Z* height of 25.4mm. On the top plane where the *Z* value is equal to 25.4mm, the scanning area is set at 25×25mm to ensure sufficient accuracy. When a surface is outside the scanning range, either the scanner or the workpiece is moved. Accordingly, the related transforming matrix can be applied to the scanning result.

Calibration of 2D Camera

Camera calibration is required for identifying the intrinsic and extrinsic parameters of a CCD camera. Hence the relation between the captured 2D image and the 3D position of a point *P* can be established. The camera calibration is a time-consuming task despite the availability of some camera calibration toolbox. For example, Zhang [15] introduced a camera calibration method, which is used in the OpenCV image processing library and many other toolboxes. However, the calibrated camera parameters and related computation models cannot fully capture the nonlinearity in a working volume.

To capture such nonlinearity for improved accuracy, the working volume (refer to Figure 5) is subdivided into 11 layers with a distance of 2.54mm between two neighboring layers in our study. A printed chessboard is fixed on the platform, which can be moved in the Z axis. Accordingly the 11 layers from z=0mm to z= 25.4mm with $\triangle z$ =2.54 mm can be calibrated separately.

For a layer K at height z_w, all the corners on the chessboard have known coordinates (x_w, y_w, z_w). An image of the chessboard is captured. Based on it, the image coordinates (X_i, Y_i) of all the corners can be identified. Accordingly the relationship between an image coordinate of each layer and the related world coordinate can be established as: $(X_i, Y_i)_{Layer\_K} = P(x_w, y_w, z_w)$. By repeating the process, a database between the 3D points within the working volume and the image points that are captured by the camera can be built as:

$$(X_i, Y_i)_{Layer\_K} = P_K(x_w, y_w, K \times \Delta z), 0 \le K \le 10. \qquad (1)$$

Such relations combine both intrinsic and extrinsic matrixes of the camera. Since the layer distance is small, a bilinear interpolation approach is used to approximate the world coordinates (x, y, z) based on two neighboring calibrated planes $P_K(x, y, K\times\Delta z)$ and $P_{K+1}(x, y, (K+1)\times\Delta z)$, when $z \in [K \times \Delta z, (K+1) \times \Delta z]$, and the four corners of a checker box.

Calibration of Laser Scanning Lines

The rotation angles of the mirror are controlled by the output values (*NS* and *WE*) provided by two Digital-Analog-Converters (DAC) in a control board. To eliminate the DAC output noises and other hardware construction errors, the laser line positions for different signal values need to be calibrated.

Different from the camera calibration, the reflected laser line is straight from the top to bottom planes. Consequently, a signal value (*NS*, *WE*) can be calibrated by the laser dots on the top and bottom planes that define a laser line. As shown in Figure 7, suppose (x_{i_10}, y_{i_10}) and (x_{i_0}, y_{i_0}) are the image position of a laser dot on the top and bottom planes. The world positions of the laser points (X_{w_10}, Y_{w_10}, Z_{w_10}) and (X_{w_0}, Y_{w_0}, Z_{w_0}) can uniquely define the laser line inside the scanning volume.

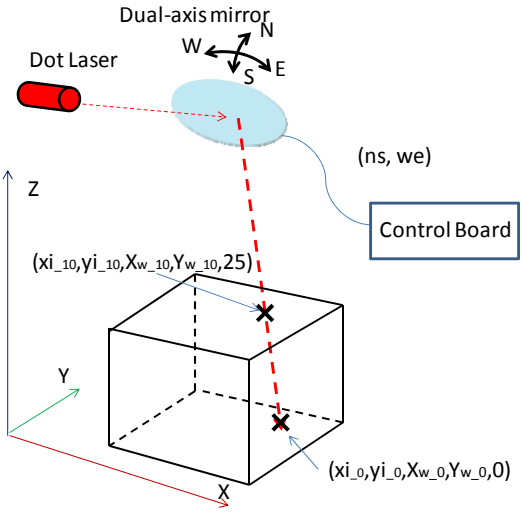

Figure 7: Laser calibration using the top plane (layer 10) and the bottom plane (layer 0).

A database consists of the positions of all the laser lines and the related DAC signal values can be built as follows:

$f(NS, WE) = (X_{w\_0}, X_{w\_10}, Y_{w\_0}, Y_{w\_10}, 0, 10\times\triangle z)$,

where *NS* and *WE* are the DAC numbers of the two axes of the mirror. The right handed side is the related world positions of the laser line on the bottom and top planes. Since a related laser line is straight, a intersection point at a level Z can be computed by the linear interpolation between the two points, L_0, and L_{10}, as recorded in the database.

Computing 3D Points

In the scanning process, the dual-axis mirror is rotated based on a given DAC number (*NS*, *WE*). The laser is first turn off to capture an image of the scanned object (without the laser dot). The laser is then turned on for capturing an image with the laser dot. Consequently, an image with the laser dot can be obtained by subtraction between the two images. Let (X_i, Y_i) denotes the image position of the laser dot. Accordingly, a set of world coordinate points $P_K(x_w, y_w, z_w)$ related to (X_i, Y_i) for each layer $K\times\Delta z$ can be identified from the camera calibration database (refer to Equation 1). Ten camera line segments P_iP_{i+1} can be computed by linear interpolation.

Similarly, the corresponding laser line related to the current DAC number (*NS*, *WE*) can be identified through the laser point calibration database. Accordingly, the laser points L_iL_{i+1} can be calculated by linear interpolation. As shown in Figure 8, the eleven layers divide the working volume into ten regions. Each region contains a camera line segment and a laser line segment. The closest point between the two line segments can be calculated in each region. For example, X_0 and X_{10} are the closest point in regions Layer0-1 and Layer9-10, respectively. The point with the smallest distance is selected as the object point in the 3D space. For example, as shown in Figure 8, X_4 in region Layer4-5 would be the computed 3D position.

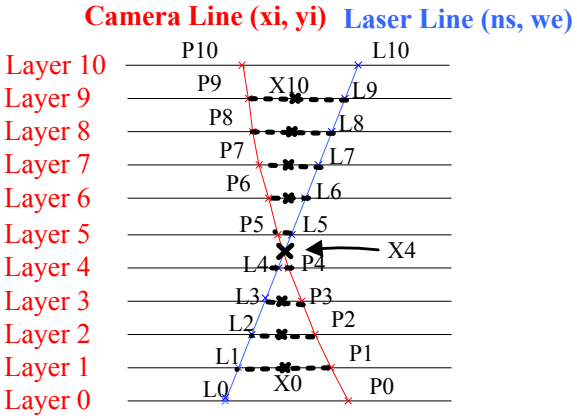

Figure 8: Point retrieval by calculating the closest point between a laser line (L_0-L_{10}) and camera line segments (P_iP_{i+1}). Laser points L_0 and L_{10} are calculated by (*ns*, *we*); camera points P_0-P_{10} are calculated by the image position of the laser dot (X_i, Y_i).

3D Scanning Verification

The aforementioned calibration databases for both camera and laser have been built. Based on them, scanning tests are performed to verify the accuracy of the developed 3D scanning system. In the first test, the platform was raised by the *z*-stage to different heights (0.0mm, 2.54mm, and 5.08mm). The planar surface is scanned and reconstructed based on the calibration databases. In the second test, a mechanical part with a height of around 3.8mm was positioned at a height of ~3.9mm. Its top surface is a planar plane. The scanning results of its top surface are recorded. Figure 9.a is the computed scanning points related to the average plane. Figure 9.b shows the deviation of all the points on the Z axis.

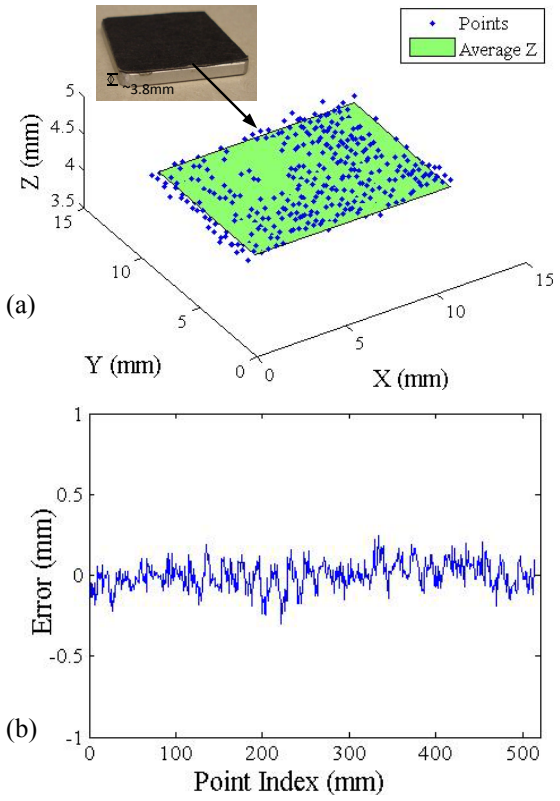

Figure 9: Scanning results of the top surface of a mechanical part. (a) Distribution of scanning points – all the points under the average Z plane are hidden; (b) deviation of all the scanning points on the Z axis.

Table 1: Statistical analysis of scanning tests

Test	Median (mm)	AVG (mm)	Max (mm)	Min (mm)	VAR (mm)
1.Platform (z = 0)	0.202	0.203	0.487	0.0	0.0075
2. Platform (z = 2.54)	2.814	2.816	3.319	2.515	0.014
3. A part (z = 3.9)	4.148	4.146	4.393	3.844	0.007
4. Platform (z = 5.08)	5.080	5.072	5.080	4.934	0.0005

Table 1 presents the statistics of the scanning results of the verification study. The average errors of the computed 3D points in the four test cases are less than 0.3mm. The scanning errors may come from the sources such as the resolution of the webcam, the control resolutions of the dual-axis mirror, and the errors in the line segment approximation and the laser dot computation. They are discussed in more details as follows.

(1) A low-cost webcam is used in the prototype system. The camera has a limited resolution of 640×480 pixels. In our setup, it is about 0.18mm/pixel. In addition, the brightest image position of the laser dot is used to represent the laser dot. Both camera resolution and the image point identification may introduce error in the final scanning result.

(2) Two digital analog convertors (DAC) are used in controlling the voltage and current of the coils that drive the dual-axis mirror. The resolution of the DAC in our control board limits the rotation resolution of the mirror. In addition, there may be vibration and other mechanical noises in the hardware setup.

(3) The laser dot used in our system has a certain focus distance. The spot size slightly changes from the top to bottom planes. In addition, the linear interpolation between two neighboring camera points may also introduce errors.

Approaches, such that adopting a better camera, using more layers in building the calibration database, and computing 3D points based on non-linear interpolation, can be developed to further reduce the scanning error. Nevertheless, the experimental results show that the scanning error of the developed 3D scanner is generally less than 0.5mm in the *Z* axis. Such accuracy is satisfactory for the CNC accumulation process. More scanning tests are given in Section 6.

4. PROCESSING OF SCANNING POINTS

The scanning results obtained by the developed 3D scanner have the following properties. (1) The sampling points can be sparse with only a small number of key points on the surface to reduce scanning time. (2) The point clouds of a surface may have uneven densities and even small holes in some areas. (3) The scanning result can be a portion of a surface. (4) The scanning results may be distorted due to measurement noises. (5) A base surface to be scanned is usually continuous since the CNC accumulation tool path is usually a set of continuous curves.

Hence a 3D surface reconstruction method that can process sparse sampling points of a continuous surface is required in the point processing software system. The algebraic point set surfaces (APSS) algorithm proposed by Gross *et. al.* [16] is a good choice in handling high curvatures and sparse point cloud. Based on an extended APSS algorithm, the layered depth-normal image (LDNI) representation presented by Wang and Chen [17] is used in generate triangular meshes of the scanned surface. Figure 10 shows the framework of the developed point processing method. The scanning data computing process is divided into the following steps: (1) preprocessing points including denoising, normal estimation, and orientation propagation; (2) constructing an implicit surface based on the APSS projection; and (3) generating sampling points of the implicit surface for constructing triangular meshes. Each step is described in details below.

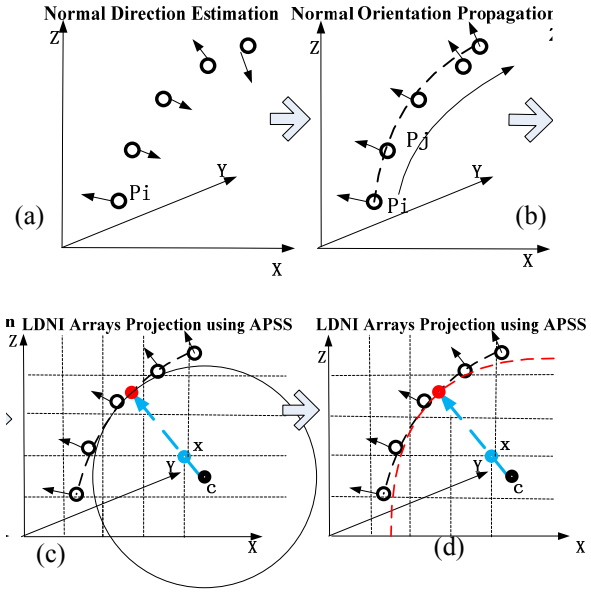

Figure 10: Overview of the point processing framework. (a) Estimation of the normals at point $\boldsymbol{p_i}$; (b) propagation of a consistent normal orientation from $\boldsymbol{p_i}$ to $\boldsymbol{p_j}$; (c) projection of a LDNI point $\boldsymbol{x}$ onto the APSS: blue point denotes query point $\boldsymbol{x}$, red point denotes the projection of $\boldsymbol{x}$, and the circle center is $\boldsymbol{c}$; (d) an illustration of the projection surface (shown in red line).

Preprocessing Scanning Points

Normal estimation and orientation play an important role in the mesh surface reconstruction. For a given set of sampling points, normal is chosen as the eigen-vector corresponding to the smallest eigen-value. It can be computed by the co-variant matrix of points:

$$\sum_{p_i \in N'(p)} (p_i - \bar{p})(p_i - \bar{p})^T \cdot \qquad (2)$$

where $N'(p)$ is the point set of the k nearest neighbors of a query point p.

However, the eigen-vector analysis cannot guarantee a correct orientation. Re-orienting the normal vectors is necessary based on a direct flipping strategy. The orientation of p_i is flipped by the closest point:

$$n_i = -n_i, if\ n_{cpi} \bullet n_i < 0 \qquad (3)$$

Algebraic Point Set Surface (APSS) Algorithm

Algebraic Point Set Surfaces algorithm is a newly developed point set surface definition based on *moving*

least squares (MLS) fitting of algebraic spheres. The surface representation can be expressed by either a projection procedure or in implicit form. Compared to existing planar MLS, the key advantages of the APSS approach include significantly improved stability of the projection under low sampling rates and in the presence of high curvature. The method can approximate or interpolate the input point set and naturally handle planar point clouds. The following weighting function is used in the fitting process [16]:

$$w_i(x) = f(\frac{\| p_i - x \|}{h_i(x)}),\ h_i(x) = K \bullet \overline{D},\ f(x) = \begin{cases} (1-x^2)^4; x<1 \\ 0; otherwise. \end{cases}$$

where $\boldsymbol{p_i}$ is a point in the input point set and $\boldsymbol{x}$ is a query point that is near the surface; $w_i(x)$ represents the weight of the point $\boldsymbol{p_i}$ for the query point $\boldsymbol{x}$; $h_i(x)$ is defined by a constant factor K timing the average distance $\overline{D}$ of $\boldsymbol{p_i}$'s k nearest neighbors. The weighting function f is a smooth and decreasing function. The weighting function proposed in [16] is used in our study.

An algebraic sphere is defined as the 0-isosurface of the scalar field $S_v(x) = [1, x^T, x^T x] \bullet V$, where $V = [v_0, ..., v_{d+1}]^T$ is the vector of scalar coefficients to describe the sphere. For $v_{d+1} \neq 0$, the corresponding center $\boldsymbol{c}$ and radius R can easily be computed [16]:

$$O = -\frac{1}{2v_{d+1}}[v_1, ..., v_d]^T, \text{ and } R = \sqrt{O^T O - v_0 / v_{d+1}}; \quad (4)$$

with d being the dimension.

In degenerate cases, $\boldsymbol{V}$ corresponds to the coefficients of a plane equation with v_0 representing the plane's distance from the origin and $[v_1, \ldots, v_d]^T$ being its normal. With normal constraints, $\boldsymbol{V}(x)$ can be computed by the following equations [16]:

$$V(x) = C^{-1}(x)\hat{b}(x), \quad (5)$$

$$C(x) = D^T W(x) D;\ \hat{b}(x) = D^T W(x) b. \quad (6)$$

$$W(x) = \begin{bmatrix} w_i & \cdots & 0 \\ 0 & \beta w_i & \vdots \\ \vdots & & \ddots & \vdots \\ 0 & 0 & & \beta w_i \end{bmatrix}; D = \begin{pmatrix} & & \\ 1 & p_i^T & p_i^T p_i \\ 0 & e_0^T & 2e_0^T p_i \\ \vdots & \vdots & \vdots \\ 0 & e_{d-1}^T & 2e_{d-1}^T p_i \end{pmatrix}; b = \begin{bmatrix} 0 \\ e_0^T n_i \\ \vdots \\ e_{d-1}^T n_i \end{bmatrix};$$

where $\{e_k\}$ represent the unit basis vectors of the coordinate system. Scalar β should be carefully chosen to weight the normal constraints. In our study, it is calculated based on: $\beta = 10^6 \times \frac{\sum_i w_i(x) h_i(x)}{\sum_i w_i(x)}$

The LDNI representation [17] is selected for converting the implicitly defined APSS surface into triangular meshes. An "almost" orthogonal projection [18] is used in computing a LDNI point. That is, the coordinate of a query point used in the LDNI projection procedure is calculated as following:

$$x'_0 = \min Ext(0) + I_x \times \Delta x; \quad (7)$$

$$x'_1 = \min Ext(1) + I_y \times \Delta y; \quad (8)$$

$$x'_2 = \min Ext(2) + i \times \Delta z; \quad (9)$$

$$\Delta z = ceil(\max Ext(2) - \min Ext(2)) / (s-1)$$

$$\vec{n} = (\vec{x} - \vec{c}) / r \quad (10)$$

where Δx, Δy denote resolutions in the X and Y directions, respectively. $\min Ext(0)$, $\min Ext(1)$, and $\min Ext(2)$ represent the minimum value of the X, Y, and Z coordinates of the input point set. $\max Ext(2)$ represents the maximum value of the Z coordinate of the input point set. I_x, I_y are the index of the X and Y axis, respectively. S is the number of points per ray, and i is an integer between 0 and S.

Figure 11 shows the LDNI-based APSS projection algorithm.

Input:
(1) A non-empty point set P={$\boldsymbol{X}$, $\boldsymbol{n}$}, which contained preprocessed scanning points $\boldsymbol{X}$, and its normal vector $\boldsymbol{n}$. Both $\boldsymbol{X}$ and $\boldsymbol{n}$ are 3 dimensional vectors;
(2) LDNI resolutions Δx, Δy in the X and Y directions, respectively; and the number of LDNI query points per ray S;
Output:
A set of points and normals (Ps and Ns) that describe a projected surface.
Steps:
(1) A point set P'={$\boldsymbol{X'}$}, where $\boldsymbol{X'}$ is a 3 dimensional query point calculated using Equations (7) to (9). Set K be the number of points in $\boldsymbol{P'}$.
(2) Set Ps={}; Ns={}; ε =0.000001;
(3) j=0;
(4) Repeat until $j = K$
(4.1) set $\boldsymbol{X'}$= $P'[j]$;
(4.2) Compute $\boldsymbol{V(X')}$ using Equation (5);
(4.3) If ($v_4 < \varepsilon$) go to plane fitting (4.3.1); else go to sphere fitting (4.3.2)
(4.3.1) Plane fitting:
(4.3.1.1) p($\boldsymbol{X'}$)= (v_0 ·v_1, v_0·v_2, v_0·v_3);
(4.3.1.2) n($\boldsymbol{X'}$)= (v_1, v_2, v_3); normalize n($\boldsymbol{X'}$);
(4.3.1.3) $\boldsymbol{X''} = \boldsymbol{X'} - n(\boldsymbol{X'})^T \times (p(\boldsymbol{X'}) - \boldsymbol{X'}) \times n(\boldsymbol{X'})$;
(4.3.1.4) If $||n(\boldsymbol{X'})^T \times (p(\boldsymbol{X'}) - \boldsymbol{X''})|| < \varepsilon$, save $\boldsymbol{X''}$ to Ps and n($\boldsymbol{X'}$) to Ns; else, go back to (4.2).
(4.3.2) Sphere fitting:
(4.3.2.1) Compute $\boldsymbol{O}$ and R using Equation (4);
(4.3.2.2) $\boldsymbol{X''} = (R / ||\boldsymbol{X'} - \boldsymbol{O}||) \cdot (\boldsymbol{X'} - \boldsymbol{O}) + \boldsymbol{O}$;
(4.3.2.3) If $||\boldsymbol{X''} - \boldsymbol{X'}|| < \varepsilon$, compute n($\boldsymbol{X''}$) using Equation (10), save $\boldsymbol{X''}$ to Ps and n($\boldsymbol{X''}$) to Ns.
else, go back to (4.2).
(4.4) $j = j+1$;
(5) output Ps and Ns.

Figure 11: Framework of the APSS fitting using the LDNI array points.

5. CNC ACCUMULATION TOOL PATH PLANNING

Tool path planning is one of the most critical steps in the machining processes such as CNC milling. Extensive research has been performed in the area with various tool path planning algorithms developed. Many commercial software systems such as *MasterCAM*, *Unigraphics*, *GibbsCAM*, and *Powermill*, are available for the CNC machining tool path planning. However, multi-axis tool path planning for additive manufacturing processes have not been well studied. Previous efforts (e.g. [19-21]) are mainly developed for the metal-based AM processes such as the Laser-aided Metal Deposition and Laser Engineered Net Shaping processes.

The tool path planning is equally important for the multi-axis CNC accumulation process. Similarity between the CNC machining and accumulation processes exists on the tool path planning. (1) Both processes require a tool or a set of tools to manipulate materials. The subtractive process removes material using the cutter while the accumulation process adds material using the curing tool. (2) The tools in both processes move along a predefined trajectory (i.e. tool path) for forming desired geometry. (3) The incremental distance of the tool path is decided by the tool size (i.e. the diameter of the tool tip for the subtractive process, and the LED spot size for the accumulation process). (4) Both processes have a fabrication depth. For subtractive processes, the cutting depth is determined by the cutter shape, the material property of the work piece, and the requirements on surface quality and building speed. For the accumulation process, the curing depth is mainly determined by the material property of the resin, the energy of the UV light source, and the bounding force between the tool and the base surface. (5) The planned tool paths in both processes should avoid collision with the workpiece.

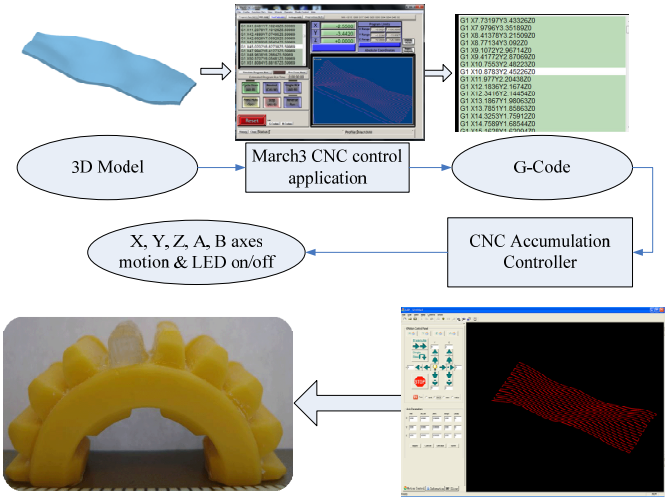

Figure 12: Tool path generation and CNC controller.

Based on the scanned surface and the CAD model of the to-be-added geometry, a general tool path planning method for the 5-axis CNC accumulation processes is developed. The method consists of the following major steps. (1) Thicken the scanned surface by using an offsetting operation with an offset distance determined by the curing depth of the tool. A general offsetting method for an input polygonal model and an arbitrary offset distance is presented in [22]. (2) Subtract the target geometry and the offset model to compute the shape of a thin layer. Robust Boolean operations based on the Layered Depth-Normal Image (LDNI) are described in [17]. (3) Generate a set of contours to fill the computed layer shape with an interval distance defined by the curing spot size. (4) Use an off-the-shelf CNC machining software system to generate numeric control G-code based on the planned tool path. (5) Use a CNC accumulation controller to load the generated G-code, and accordingly send motion commands to a controller to drive the 5-axis motion. At the same time, a micro-controller is used to control the curing state (i.e. turning the LED ON/OFF). Figure 12 illustrates the aforementioned steps with two more examples presented in Section 6.

6. EXPERIMENTAL RESULTS

Based on the planned tool paths, accumulation tools can selectively cure liquid resin into desired shape on the scanned surface. Two test cases were designed to verify the effectiveness of the developed CNC accumulation system on building around inserts.

Experimental Setup

The hardware setup of our prototype system is shown in Figure 6. The 5-axis motion configuration of an accumulation tool is shown in Figure 13. The tool is mainly based on using a light guide to provide UV light from a LED to the tip of the fiber optics. Based on our previous study [4], a Teflon film is also applied on the tool tip as the coating media. A 5-axis motion system including *X*, *Y*, *Z* translations and *A*, *B* rotations is designed to allow the tool to cure resin in various positions and orientations.

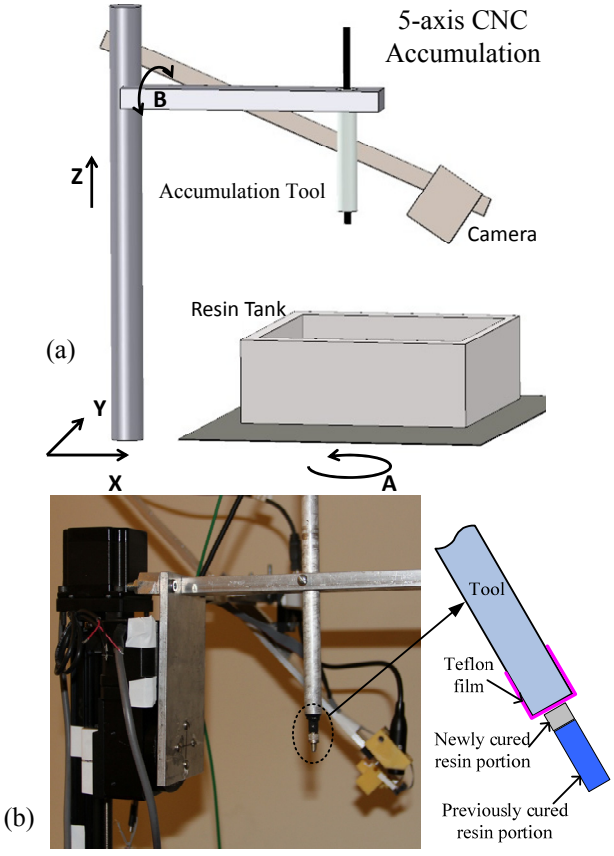

Figure 13: Multi-axis motion configuration of the CNC accumulation system. (a) A schematic drawing; (b) an illustration of an accumulation tool used in the system.

During the building process, an inserted component is mounted on a resin tank that is placed on the platform. The surface to be used as the base is scanned by the developed 3D scanner. The tank is then filled with UV curable resin. The building process can then start after the tool paths have been planned. After the accumulation process finishes, the built object is taken out for post-processing.

Repairing a Broken Gear

A test case on repairing an existing plastic part is shown in Figures 14 and 15. In the test, a gear was built using a commercial SLA machine. We manually break one tooth of the gear (refer to Figure 14a). Note that the broken surface on which material will be deposited is irregular. With the integrated CNC accumulation system, it is possible to repair the broken gear.

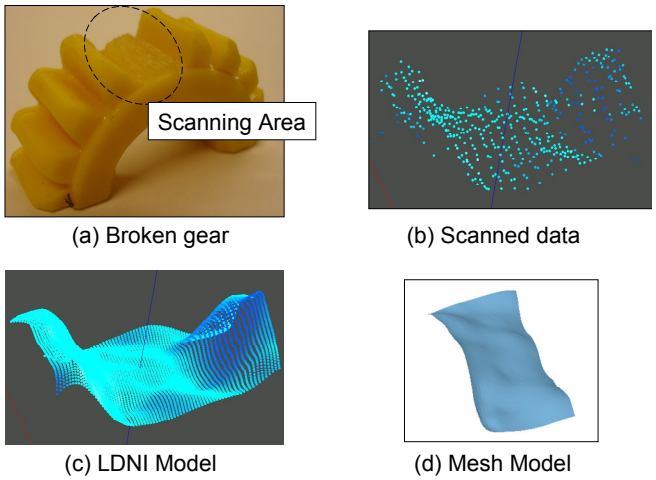

Figure 14: Surface reconstruction for the CNC accumulation process. (a) A broken part; (b) scanning points of the broken surface; (c) generated LDNI points based on the APSS-LDNI fitting of the scanning points; (d) the base surface model generated from the LDNI points.

First, the working surface, on which a new tooth will be built, is scanned. As shown in Figure 14b, the scanning point set is sparse with noises. The scanning points are processed using the point processing algorithms as described in Section 4. The computed LDNI point set after the point processing step is shown in Figure 14c. Finally a triangular mesh as shown in Figure 14d is constructed from the LDNI model.

Assuming the scanned surface has been aligned with the target CAD model (refer to Figure 15a). A set of offsetting operations can be performed based on the scanned surface and a given curing depth. Accordingly multiple layers can be computed based on the offset models and the target tooth model. As shown in Figure 15b, there are 15 layers to be built in order to repair the missed tooth. Note all the layers have a uniform thickness. For each layer, continuous tool paths can be planned based on the layer model as shown in Figure 14d. Figure 15c shows the tool path of one layer in the CNC accumulation process. Note that the planned tool path is not on a planar plane, which requires 5-axis motions. Based on the planned tool paths, the repairing work of the broken gear can be performed by the CNC accumulation process. Figure 15d shows the repaired gear. For demonstration purpose, a different resin is used in the CNC accumulation process. If the same type of resin was used, the repaired tooth would be the same as other teeth.

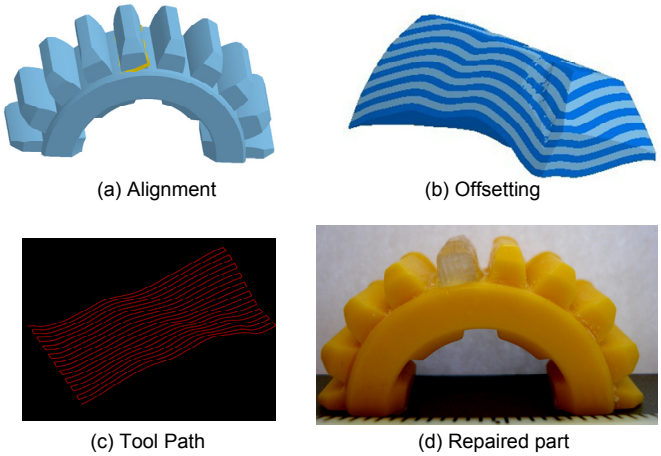

Figure 15: Fabrication process based on a scanned surface. (a) Alignment of the surface with the gear model; (b) offsetting results for 15 accumulation layers; (c) the tool path of a layer; (d) the repaired gear.

Modifying a Curved Surface

As mentioned before, each manufacturing process has its own advantages and disadvantages. For example, complex geometries such as surface textures and characters are difficult to be fabricated by forming processes such as injection molding and extrusion. Such complex features will significantly increase the tooling cost in the forming processes. Assume a teapot with no surface textures or characters is fabricated by the injection molding process (refer to Figure 16a). Due to the lack of injection molding tools, the model was still fabricated by a SLA machine in the test. Such simple geometry can be efficiently fabricated by the forming process with much lower cost. However, the final component may have complex features that are difficult to be injection molded. For adding such features, the integrated CNC accumulation system can be used in modifying an existing part that is fabricated by other manufacturing processes.

Assume on the smooth exterior surface of the teapot, some characters such as “USC” are required. Similar to the previous test case, the portion of the surface where the new feature will be added is scanned. The scanning result is shown in Figure 16b. The scanning points are then processed by the point processing algorithms as described in Section 4. A much smoother and denser LDNI point set is generated as shown in Figure 16c. A mesh surface can be constructed from the LDNI points (refer to Figure 16d).

Assume the CAD model of "USC" pattern and its position on the scanned surface are known (refer to Figure 17a). Accordingly related layers of the "USC" pattern can be computed by offsetting the pattern surface (refer to Figures 17b). The corresponding tool paths for each layer can be generated as shown in Figure 17c. The teapot modified by the integrated CNC accumulation system is shown in Figure 17d. Note in such a component, two different manufacturing processes have been used in its fabrication. Each process utilizes its unique properties. That is, the injection molding processes is fast and low-cost; while the CNC accumulation process is capable of fabricating complex shapes on arbitrary surfaces.

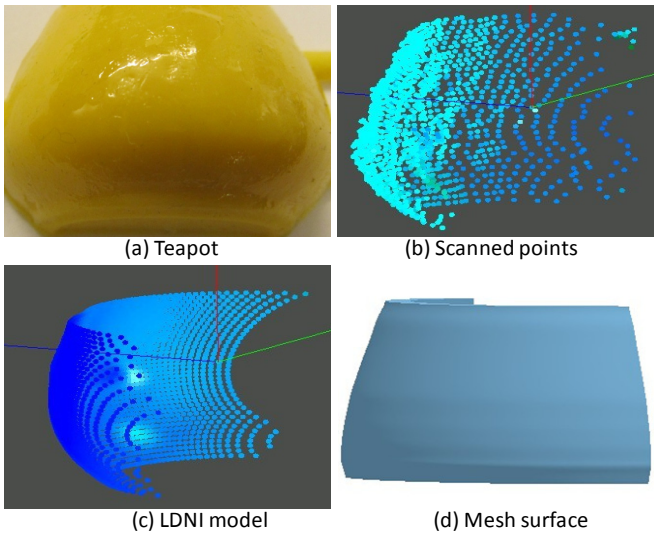

Figure 16: Scanning and post processing of the scanned surface. (a) An existing teapot. (b) Scanned points. (c) LDNI model. (d) Mesh surface.

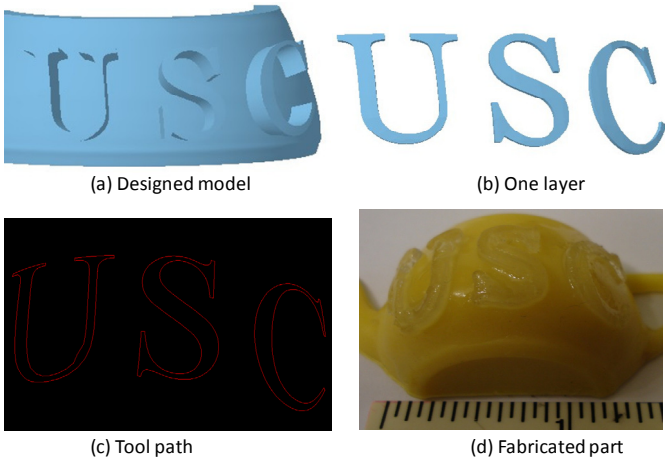

Figure 17: The tool path and fabricated part. (a) The designed model; (b) a sliced layer; (c) the tool path of a layer; (d) the fabricated object by two manufacturing processes.

7. CONCLUSION AND FUTURE WORK

Building-around-inserts is an important issue for future direct digital manufacturing research and development. An integrated CNC accumulation process has been developed based on a novel 3D laser scanning system that uses a dual-axis mirror. Compared to conventional laser scanning systems, the use of the MEMS device increases the scanning freedom of the system from one-dimensional line segment to a two-dimensional surface area. Related point processing algorithms have also been developed based on the APSS fitting and the LDNI representation. Experiments verify the accuracy and compactness of the 3D scanning system. The 3D scanner has also been integrated in a 5-axis CNC accumulation system. Experimental results illustrate the capability of the integrated CNC accumulation process on building-around-inserts. Its applications on plastic part repairing and modification may provide solutions for future development on sustainable manufacturing and heterogeneous component design.

Considerable work remains to mature the developed AM process and the related prototype system. Some current work we are investigating include exploring new applications of the 3D scanning system, developing more accumulation tools with higher speed and resolution, and extending the multi-axis CNC accumulation process into micro-scale fabrication.

REFERENCES

[1] Kalpakjian, S. and Schmid S. R., 2010, *Manufacturing Engineering and Technologies*, Pearson Prentice Hall, 6th Edition.

[2] Kataria A., Rosen D. W., 2001. Building around inserts: methods for fabricating complex devices in stereolithography. *Rapid Prototyping Journal*, 7(5):253-62.

[3] Campbell I., Bourell D., Gibson I., 2012. Additive manufacturing: Rapid prototyping comes of age. *Rapid Prototyping Journal*, 18(4):255-8.

[4] Chen Y., Zhou C., Lao J., 2011. A layerless additive manufacturing process based on CNC accumulation. *Rapid Prototyping Journal*, 17(3):218-27.

[5] Jocobs, F. P., 1992, *Rapid prototyping and manufacturing: fundamentals of Stereolithography*, Society of Manufacturing Engineers, Dearborn, MI.

[6] Pan, Y., C. Zhou, Y. Chen, 2012, A fast mask projection Stereolithography process for fabricating digital models in minutes. *ASME Journal of Manufacturing Science and Engineering*, Vol. 134, No. 5, pp. 051011.

[7] Chen F., Brown G, Song M., 2000. Overview of three-dimensional shape measurement using optical methods. *Optical Engineering*, 39(1):10.

[8] Forrest, A. K., 2012, Laser scanners, *Machine Vision Handbook*, Batchelor, B. (Ed.), Springer, pp. 329-54.

[9] Golnabi H., 2000. Design and operation of a laser scanning system. *Optics and Laser Technology*. 32(4):267-72.

[10] Abuazza A, Brabazon D, El-Baradie MA., 2003. Analysis of surface defects using a novel developed fiber-optics laser scanning system. *Journal of Materials Processing Tech*. 143:875-9.

[11] Li Y., 2008. Beam deflection and scanning by two-mirror and two-axis systems of different architectures: A unified approach. *Applied Optics*. 47(32):5976-85.

[12] Golnabi H., 1999. Image evaluation for the synchronised laser scanning systems. *Optics and Laser Technology*. 31(3):225-32.

[13] Zhou, C., Chen, Y. 2012. Additive manufacturing based on optimized mask video projection for improved accuracy and resolution." *SME Journal of Manufacturing Processes*, 14(2): 107-118.

[14] Texas Instruments Inc., retrieved Nov. 15, 2012, http://www.ti.com/product/talp1000b.

[15] Zhang Z., 1999. Flexible camera calibration by viewing a plane from unknown orientations. *International Conference on Computer Vision* (ICCV'99), Corfu, Greece, pages 666–673.

[16] Gross M., Guennebaud G, Zurich E., 2007. Algebraic point set surfaces. *ACM Transactions on Graphics*, 26(3).

[17] Wang, C. C. L., Leung, Y., Chen, Y., 2010, Solid modeling by Layered Depth-Normal Images on the GPU." *Computer-aided Design*, 42(6): 535-544.

[18] Alexa M., Adamson A., 2004. On normals and projection operators for surfaces defined by point sets. In *Proceedings of the Eurographics Symposium on Point-Based Graphics*, 149-156

[19] Sundaram R, Choi J., 2004. A slicing procedure for 5-axis laser aided DMD process. *ASME Journal of Manufacturing Science and Engineering*. 126(3):632.

[20] Zhang J., 2004. Adaptive slicing for a multi-axis laser aided manufacturing process. *ASME Journal of Mechanical Design*. 126(2):254.

[21] Ruan J, Eiamsa-ard K, Liou FW., 2005. Automatic process planning and tool path generation of a multi-axis hybrid manufacturing system. *ASME Journal of Manufacturing Processes*. 7(1):57-68.

[22] Chen Y, Wang C. C. L., 2011. Uniform offsetting of polygonal model based on layered depth-normal images. *Computer-Aided Design*, 43(1):31-46.